bioRxiv preprint doi: https://doi.org/10.1101/422246; this version posted September 19, 2018. The copyright holder for this preprint (which was not certified by peer review) is the author/funder, who has granted bioRxiv a license to display the preprint in perpetuity. It is made available under aCC-BY-NC-ND 4.0 International license.

Theta-Gamma Cascades and Running Speed

Abbreviated Title: *Theta-Gamma Cascades*

A. Sheremet[1,2], J.P. Kennedy[1*], Y. Qin[2*], Y. Zhou[2*], S.D. Lovett[1], S.N. Burke[1,3], A. P. Maurer[1,2,4]

[1]McKnight Brain Institute, Department of Neuroscience, University of Florida, Gainesville, FL. 32610.
[2]Engineering School of Sustainable Infrastructure and Environment, University of Florida, Gainesville, FL. 32611.
[3]Institute of Aging, University of Florida, Gainesville, Florida 32603.
[4]Department of Biomedical Engineering, University of Florida, Gainesville, FL. 32611.

[*]These authors contributed equally to this work

Correspondence: Drew Maurer
McKnight Brain Institute,
1149 Newell Dr., RM L1-100E
University of Florida
Gainesville, Florida 32610
Tel: (352) 273-5092
Email: drewmaurer@ufl.edu

Number of pages: 36
Number of figures: 9
Number of tables: 0
Abstract words: 213
Introduction words: 637
Discussion words: 1688

The authors declare no conflict of interest.

Key words: Coupling, Memory, Cognition, Rat, Criticality

Acknowledgements: This work was supported by the McKnight Brain Research Foundation, and NIH grants- Grant Sponsor: National Institute on Mental Health; Grant Number: R01MH109548 and a Diversity Supplement to NIH grant R01MH109548 (JPK). We would like to thank Drs. Gyuri Buzsaki, Kamran Diba and Eric Schomburg for comments on an earlier draft of the manuscript.

bioRxiv preprint doi: https://doi.org/10.1101/422246; this version posted September 19, 2018. The copyright holder for this preprint (which was not certified by peer review) is the author/funder, who has granted bioRxiv a license to display the preprint in perpetuity. It is made available under aCC-BY-NC-ND 4.0 International license.

Abstract

The local field potentials (LFPs) of the hippocampus are primarily generated by the spatiotemporal accretion of electrical currents via activated synapses. Oscillations in the hippocampal LFP at theta and gamma frequencies are prominent during awake-behavior and have demonstrated several behavioral correlates. In particular, both oscillations have been observed to increase in amplitude and frequency as a function of running velocity. Previous investigations, however, have examined the relationship between velocity and each of these oscillation bands separately. Based on energy cascade models where "…*perturbations of slow frequencies cause a cascade of energy dissipation at all frequency scales*" (Buzsaki 2006), we hypothesized that the cross-frequency interactions between theta and gamma should increase as a function of velocity. We examined these relationships across multiple layers of the CA1 subregion and found a reliable correlation between the power of theta and the power of gamma, indicative of an amplitude-amplitude relationship. Moreover, there was an increase in the coherence between the power of gamma and the phase of theta, demonstrating increased phase-amplitude coupling with velocity. Finally, at higher velocities, phase entrainment between theta and gamma becomes stronger. These results have important implications and provide new insights regarding how theta and gamma are integrated for neuronal circuit dynamics, with coupling strength determined by the excitatory drive within the hippocampus.

bioRxiv preprint doi: https://doi.org/10.1101/422246; this version posted September 19, 2018. The copyright holder for this preprint (which was not certified by peer review) is the author/funder, who has granted bioRxiv a license to display the preprint in perpetuity. It is made available under aCC-BY-NC-ND 4.0 International license.

Introduction

The observation that changes in local field potential (LFP) oscillations correlate with the behavioral state of an animal has a long history (for review, see Buzsáki 2005). Nevertheless, the mechanisms that generate and organize oscillatory activity are still opaque. For example, it has been proposed that different LFP oscillations and their couplings support different processes and network functions (Belluscio et al. 2012; Bieri et al. 2014; Colgin et al. 2009; Gloveli et al. 2005; Lisman and Jensen 2013; Tort et al. 2009; Tort et al. 2008). However, the neurophysiological mechanisms responsible for integrating neuron spiking and oscillations across to temporal scales to support cognition have yet to be elucidated. The observation that hippocampal neuron firing rate (McNaughton et al., 1983; Maurer et al., 2005), theta power (Sheremet et al., 2016 and others) and gamma power (Ahmed and Mehta 2012; Chen et al. 2011; Kemere et al. 2013; Zheng et al. 2015) all increase with faster running speeds suggest that synaptic potentials organization across the macroscopic scale (theta) to the microscopic level of the single units. Specifically, as slow oscillations can entrain a large volume of neurons, they are in a better position to ‘coordinate’ local events (Buzsáki and Draguhn 2004). Gamma, on the mesoscopic level, is an inevitable pattern when fast excitation and inhibition compete (Buzsaki 2006; Buzsáki et al. 2004; Buzsáki and Wang 2012; Wang and Buzsáki 1996). On the microscopic scale, basket cells appear to be critical in gamma generation given their fast time course and perisomatic terminals onto pyramidal cells (Buzsaki 2006; Freund and Buzsáki 1996). Thus, during theta states, large-scale activation provides the input necessary for inhibitory and excitatory processes to compete on the mesoscale level (generating high amplitude gamma). This

bioRxiv preprint doi: https://doi.org/10.1101/422246; this version posted September 19, 2018. The copyright holder for this preprint (which was not certified by peer review) is the author/funder, who has granted bioRxiv a license to display the preprint in perpetuity. It is made available under aCC-BY-NC-ND 4.0 International license.

input is also seen on the microscopic level with interactions between interneurons and pyramidal cells.

Previously, we have demonstrated increases in single unit firing rate with rat-running velocity (Maurer et al. 2005). Furthermore, accompanying the increase in firing rate, we found changes in sequence compression (defined as the ratio of the rate of cell assembly transition to the rat's actual velocity; see Dragoi and Buzsáki 2006; Skaggs et al. 1996) at faster-running speed (Maurer et al. 2012). With respect to the LFP, these changes are accompanied by an increase in theta power, theta frequency, and the number of theta harmonics(Sheremet et al. 2016). Finally, we revealed that pyramidal cells and interneurons interact through putative monosynaptic connection to organize spike firing times (Maurer et al. 2006). Therefore, based on these findings and the role of interneurons in shaping gamma oscillations, we sought to empirically test the hypothesis that theta and gamma inevitably couple in proportion to the amount of activity into the network.

Here, we investigate the interaction between gamma (50-120 Hz; Bragin et al. 1995; Chrobak and Buzsáki 1998; Leung 1992; Penttonen et al. 1998; Stumpf 1965) and the 6-10 Hz theta oscillation (GREEN and ARDUINI 1954; Jung and Kornmüller 1938; Vanderwolf 1969) across hippocampal CA1 laminae: stratum oriens, pyramidal, radiatum and lacunosum-moleculare. Critically, these different laminae are associated with distinct afferent input. The hippocampus has a highly conserved anatomical organization with afferent input and intrinsic fiber projections terminating in discrete layers. For example, the stratum lacunosum-moleculare region of CA1 neurons receives input from the layer III of the entorhinal cortex (Witter et al. 1988), nucleus reuniens

bioRxiv preprint doi: https://doi.org/10.1101/422246; this version posted September 19, 2018. The copyright holder for this preprint (which was not certified by peer review) is the author/funder, who has granted bioRxiv a license to display the preprint in perpetuity. It is made available under aCC-BY-NC-ND 4.0 International license.

(Wouterlood et al. 1990) and amygdala (Pikkarainen et al. 1999), while the stratum radiatum and oriens receive CA3 Schaeffer collateral and commissural fibers (Hjorth-Simonsen 1973; Ishizuka et al. 1990). Concerning local projections, different populations of interneurons target distinct hippocampal lamina with parvalbumin positive cells synapsing in the stratum pyramidale and oriens while the somatostatin positive cells target the stratum lacunosum-moleculare (Freund and Buzsáki 1996). Together, these data suggest that there should be a laminar sensitivity to theta-gamma oscillatory coupling as a function of movement speed.

bioRxiv preprint doi: https://doi.org/10.1101/422246; this version posted September 19, 2018. The copyright holder for this preprint (which was not certified by peer review) is the author/funder, who has granted bioRxiv a license to display the preprint in perpetuity. It is made available under aCC-BY-NC-ND 4.0 International license.

Materials and Methods –

SUBJECTS AND BEHAVIORAL TRAINING.

All behavioral procedures were performed in accordance with the National Institutes of Health guidelines for rodents and with protocols approved by the University of Florida Institutional Animal Care and Use Committee. A total of five 4-10 months old Fisher344-Brown Norway Rats (Taconic) were used in the present study. This was a mixed sex cohort comprised of r530♂, r538♂, r544♀, r547♂ , and r695♀ in order to integrate sex a biological variable and begin to alleviate the disparity in research focused exclusively on males (Clayton 2016). In the present study, we had no *a priori* predictions that sex will alter oscillations of the hippocampus as single unit physiology is relatively consistent in female animals across estrous (Tropp et al. 2005). Upon arrival, rats were allowed to acclimate to the colony room for one week. The rats were housed individually and maintained on a 12:12 light/dark cycle. All training sessions and electrophysiological recordings took place during the dark phase of the rats' light/dark cycle. Training consisted of shaping the rats to traverse a circular track for food reward (45mg, unflavored dustless precision pellets; BioServ, New Jersey; Product #F0021). During this time, their body weight was slowly reduced to 85% to their arrival baseline. Once the rat reliably performed more than one lap per minute, they were implanted with a custom single shank silicon probe from NeuroNexus (Ann Arbor, MI). This probe was designed such that thirty-two recording sites, each with a recording area of 177 μm^2, were spaced 60 µm apart allowing incremental recording across the hippocampal lamina. In preparation for surgery, the probe was cleaned in a 4% dilution of Contrad

bioRxiv preprint doi: https://doi.org/10.1101/422246; this version posted September 19, 2018. The copyright holder for this preprint (which was not certified by peer review) is the author/funder, who has granted bioRxiv a license to display the preprint in perpetuity. It is made available under aCC-BY-NC-ND 4.0 International license.

detergent (Decon Contrad 70 Liquid Detergent, Fisher Scientific) and then rinsed in distilled water (Vandecasteele et al. 2012).

SURGICAL PROCEDURES.

Surgery and all other animal care and procedures were conducted in accordance with the NIH Guide for the Care and Use of Laboratory Animals and approved by the Institutional Animal Care and Use Committee at the University of Florida. Rats were initially sedated in an induction chamber. Once anesthetized, the rat was transferred to a nose cone. The head was shaved with care taken to avoid the whiskers. The rat was then transferred to the stereotax, gently securing the ear bars and placing the front teeth over the incisor bar. The stereotaxic nose cone was secured, ensuring that the rat was appropriately inhaling the anesthesia. During surgical implantation, the rats were maintained under anesthesia with isoflurane administered at doses ranging from 0.5 to 2.5%. Next, ophthalmic ointment was applied and “tanning shades”, fabricated out of foil, were placed over but not touching the eyes to minimize direct light exposure. Multiple cycles of skin cleaning, using betadine followed by alcohol was applied prior to the first incision from approximately the forehead to just behind the ears. The remaining fascia was blunt dissected away and bone bleeding was mitigated through application of bone wax or cautery. Once the location of bregma was determined, the site of the craniotomy was located and a 3x3mm contour was drilled out, but not completed. This was followed by the placement of 7 anchor screws in the bone as well as a reference over the cerebellum and ground screw placed over the cortex. Once the screws were secured, a thin layer of dental acrylic (Grip Cement Industrial Grade, 675571 (powder) 675572 (solvent); Dentsply Caulk, Milford, DE) was applied taking care to not obscure

bioRxiv preprint doi: https://doi.org/10.1101/422246; this version posted September 19, 2018. The copyright holder for this preprint (which was not certified by peer review) is the author/funder, who has granted bioRxiv a license to display the preprint in perpetuity. It is made available under aCC-BY-NC-ND 4.0 International license.

the craniotomy location. Finally, the craniotomy location was completed, irrigating and managing bleeding as necessary once the bone fragment was removed. Next a portion of the dura was removed, taking care to avoid damaging the vessels and the surface of the neocortex. Small bleeding was managed with saline irrigation and gel foam (sterile absorbable gelatin sponges manufactured by Pharmacia & Upjohn Co, Kalamazoo, MI; a division of Pfizer, NY, NY). The probe implant coordinates targeted the dorsal hippocampus (AP: -3.2 mm, ML: 1.5 relative to bregma, DV: -3.7 to brain surface).

Once the probe was in place, the craniotomy was covered with silastic (Kwik-Sil, World Precision Instruments, Sarasota, FL) and then secured to the anchor screws with dental acrylic. Four copper mesh flaps were placed around the probe providing protection as well as acting as a potential Faraday cage. The wires from the reference and ground screws were soldered to the appropriate pins of the connector. Adjacent regions of the coppermesh flaps were soldered together to ensure their electrical continuity and the ground wire soldered to the coppermesh taking care to isolate the reference from contact with the ground. Once the probe was secured, the rat received 10cc of sterile saline as well as metacam (1.0 mg/kg) subcutaneously (the non-steroidal anti-inflammatory is also known as meloxicam; Boehringer Ingelheim Vetmedica, Inc., St. Joseph, MO). The rat was placed in a cage and monitored constantly until fully recovered. Over the next 7 days, the rat was monitored to ensure recovery and no behavioral anomalies. Metacam was administered the day following surgery as well. Antibiotics (Sulfamethoxazole/TrimethoprimOral Suspension at 200mg/40 mg per 5 mls; Aurobindo Pharma USA, Inc., Dayton, NJ) were administered in the rat mash for an additional 5 days.

bioRxiv preprint doi: https://doi.org/10.1101/422246; this version posted September 19, 2018. The copyright holder for this preprint (which was not certified by peer review) is the author/funder, who has granted bioRxiv a license to display the preprint in perpetuity. It is made available under aCC-BY-NC-ND 4.0 International license.

NEUROPHYSIOLOGY.

Following recovery from surgery, rats were retrained to run unidirectionally on a circle track (outer diameter: 115 cm, inner diameter: 88 cm), receiving food reward at a single location. For rats 530, 544 and 695, data is only analyzed from the circle track conditions. In order to deal with low velocities from the circle track datasets, additional datasets for rats 538 and 539 from running on figure-8 track (112cm wide x 91cm length) were used. In this task, rats were rewarded on successful spatial alternations. Only datasets in which the rats performed more than 85% of trials correctly were used. The local field potential was recorded on a Tucker-Davis Neurophysiology System (Alachua, FL) at ~24kHz (PZ2 and RZ2, Tucker-Davis Technologies). The animal's position was recorded at 30 frames/s (Tucker-Davis). Spatial resolution was less than 0.5 cm/pixel.

ANALYSES AND STATISTICS.

Velocity was calculated as the smoothed derivative of position. The local field potential data was analyzed in Matlab® (MathWorks, Natick, MA, USA) using custom written code as well as code imported from the HOSAtoolbox (Swami et al. 2003). Raw LFP records sampled at 24 kHz (Tucker-Davis system) were low-pass filtered down to 2 kHz and divided into sequences of 1024 time samples (approx. 0.5 s). The analysis of the LFP in the current study was based on standard techniques used for stationary signals (Papoulis and Pillai 2002; Priestley 1981) as previously described in Sheremet et al. (2016). Briefly, we assume that the LFP time series is a stochastic process, stationary in the relevant statistics, and decompose it using the discrete Fourier

bioRxiv preprint doi: https://doi.org/10.1101/422246; this version posted September 19, 2018. The copyright holder for this preprint (which was not certified by peer review) is the author/funder, who has granted bioRxiv a license to display the preprint in perpetuity. It is made available under aCC-BY-NC-ND 4.0 International license.

209 transform (DFT). The Fourier transform time sequences were reduced to the non-
210 redundant frequency domain of 1 Hz ≤ ω ≤ 1 kHz (where ω are the analyzed
211 frequencies), with a frequency increment of 1 Hz.

212 Electrode position along the CA1-dentate axis was determined initially via visual
213 inspection of the LFP, followed by traditional current source density analyses (Bragin et
214 al. 1995; Buzsáki et al. 1986; Mitzdorf 1985; Rappelsberger et al. 1981). Shifts in the
215 phase of theta from stratum oriens to the dentate (Buzsáki et al. 1983; Leung 1984;
216 Winson 1978) as well as the regional distribution of currents – triggered on ripples –

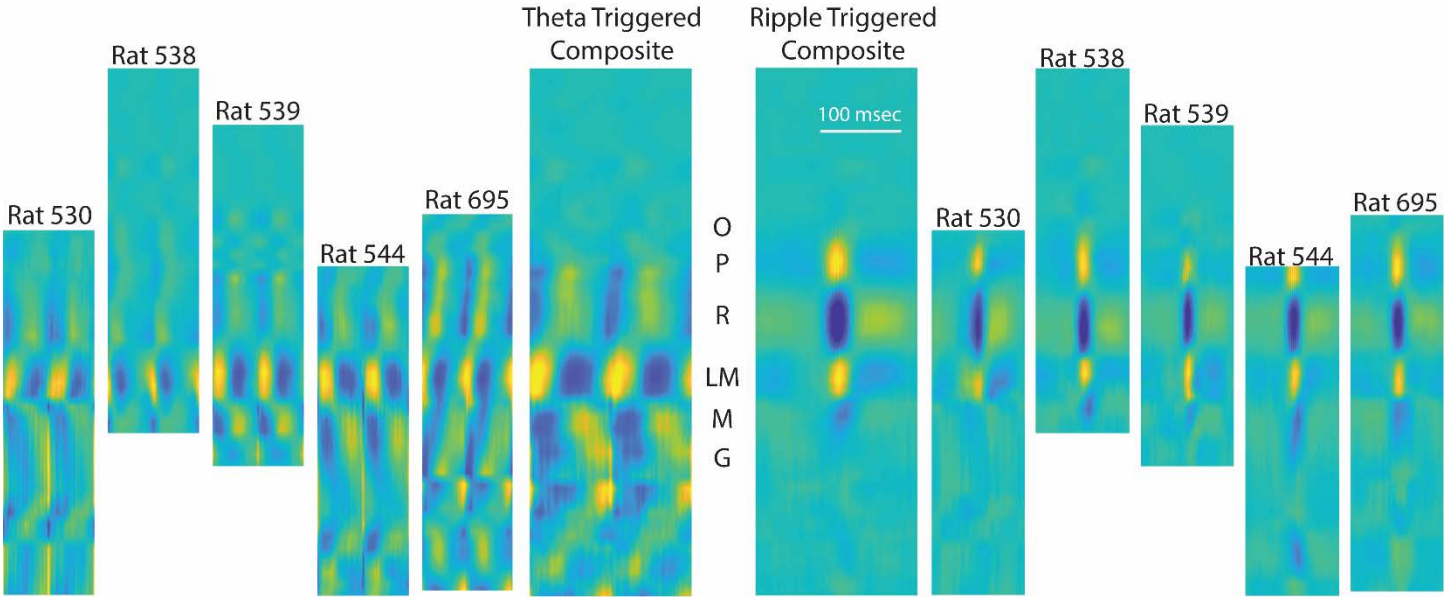

Figure 1: Using current source density for electrode localization across rats. The left side of the figure is the current source density of the raw LFP triggered on the maximum positive deflection of the filtered theta rhythm, with time normalized to two cycles of the hippocampal theta rhythm. On the right are the individual rat current source density plots for the unfiltered LFP, triggered on the maximum positive going ripple in the pyramidal cell layer (sources are warm colors, sinks are cool colors). In order to identify the layers across each rat, composite images (center) were generated with the output compared to prior publications (Bragin et al., 1995; Sullivan et al., 2011; Buzsaki, 2015). Both the theta and ripple current source density analyses were calculated during either awake-behavior or rest epochs. To account for differences in hippocampal size, the current source density images were cross-correlated with each other in order to determine appropriate alignment and compression. For the purposes of the current analyses, the oriens (O), pyramidal layer (P), stratum radiatum (R), lacunosum moleculare (LM), molecular layer (M) and upper granule layer (G) were identified.

bioRxiv preprint doi: https://doi.org/10.1101/422246; this version posted September 19, 2018. The copyright holder for this preprint (which was not certified by peer review) is the author/funder, who has granted bioRxiv a license to display the preprint in perpetuity. It is made available under aCC-BY-NC-ND 4.0 International license.

217 revealed sources and sinks that directly related to input layers (Fig. 1; Sullivan et al.
218 2011; Ylinen et al. 1995a).

219 **Power-Power Correlations**

220 To investigate the relationship between theta and gamma power, the LFP recordings
221 were down-sampled to 2 kHz and split into 1-s segments. In order to remove epochs
222 with potential noise, an LFP quality control algorithm was applied to remove segments
223 with either 1) too large or too small variance (>3*mean(variance) or
224 <0.1*mean(variance) or 2) with maximum (or minimum) LFP recording has a 10 STD
225 deviation from the mean (maximum(LFP)>mean(LFP)+10*std(LFP) or
226 minimum(LFP)<mean(LFP)-10*std(LFP)). The mean velocity for each segment was
227 computed and only segments with mean velocity larger than 5 cm/s were included for
228 this analysis. For each segment, the power spectrum was estimated with the multitaper
229 method. The first three DPSS sequences were used to get the tapered spectrum
230 estimations. Tapered spectrum estimations were computed with 2000 FFT points and
231 averaging over these spectrum estimations generated the multitaper spectrum. The
232 power of the LFP in a given frequency range is the area under the power spectrum
233 curve within that frequency range. Each observation in the power-power correlation
234 analysis is the power of theta (6-10 Hz) and gamma (50-120 Hz) for a 1-s segment.

235 **Phase-power Coherency**

236 The LFP recordings were down-sampled to 2000 Hz, split into 1-s segments, and
237 sorted according to their corresponding average velocity into 4 classes [0,5], (5,15],
238 (15,35], and >35 cm/s. If $\mathrm{X}(t)$ is a 1-s time-series segment that belongs to a given

bioRxiv preprint doi: https://doi.org/10.1101/422246; this version posted September 19, 2018. The copyright holder for this preprint (which was not certified by peer review) is the author/funder, who has granted bioRxiv a license to display the preprint in perpetuity. It is made available under aCC-BY-NC-ND 4.0 International license.

velocity class, the corresponding power time series $\mathrm{Y_{f_1}(t)}$ at frequency $\mathrm{f_1}$ was obtained by using wavelet transform. The wavelet transform decomposes $\mathrm{X}(t)$ into the time-scale domain, and $Y_{f_1}(t)$ is the modulus square of wavelet transform at the scale whose central frequency is f_1. The Fourier transforms of time series $\mathrm{X}(t)$ and $Y_{f_1}(t)$ are $\hat{X}(f)$ and $\hat{Y}(f)$, and the cross-spectrum between $\mathrm{X}(t)$ and $Y_{f_1}(t)$ is $\langle \hat{X}(f)\widehat{Y^*}(f)\rangle$ where $\langle . \rangle$ is the expected-value operator. The phase-power coherence is defined as the modulus of the cross-spectrum $\langle \widehat{X}\,\widehat{Y^*}\rangle$ normalized by the power spectra of X and Y_{f_1}, and the mathematical expression for phase-power coherence is $\left|\frac{\langle \hat{X}\hat{Y}^*\rangle}{(\langle \hat{X}\hat{X}^*\rangle\langle \hat{Y}\hat{Y}^*\rangle)^{1/2}}\right|$. Informally, the phase-power coherence measures how much the power time series of frequency component f_1 is modulated by frequency components f in the original signal.

Bispectrum and Bicoherence

The bispectrum has been thoroughly reviewed in terms of both statistical and mathematical background (Harris 1967) as well as its application to nonlinear wave interaction (Kim and Powers 1979). As noted in our prior publication (Sheremet et al. 2016) as well as others, bispectral analysis (the Fourier transform of the third order cumulant) quantifies the degree of phase coupling between the frequencies of the LFP while the bicoherence quantifies the degree of cross-frequency coupling independent from the amplitude (Barnett et al. 1971; Bullock et al. 1997; Gloveli et al. 2005; Hagihira et al. 2001; Li et al. 2009; Muthuswamy et al. 1999; Ning and Bronzino 1989; Shahbazi Avarvand et al. 2018; Sigl and Chamoun 1994; Wang et al. 2017). The utility of the bispectrum can be illustrated as follows. In the instances of “no coupling”, three independent waves – ω_1, ω_2, and $\omega_1 + \omega_2$, will have statisically independent phases

bioRxiv preprint doi: https://doi.org/10.1101/422246; this version posted September 19, 2018. The copyright holder for this preprint (which was not certified by peer review) is the author/funder, who has granted bioRxiv a license to display the preprint in perpetuity. It is made available under aCC-BY-NC-ND 4.0 International license.

relative to each other, resulting in a random phase mixing when estimated over multiple realizations. In these instances, the bispectrum will take a zero value. When three waves are nonlinearly coupled, however, a phase coherence will exist between ω_1, ω_2, and $\omega_1 + \omega_2$, resulting in a non-zero bispectral value (Fig. 2; Kim et al. 1980). In order to analyze for nonlinear phase coupling between hippocampal LFP frequencies, local field potential the datawere analyzed in Matlab® (MathWorks, Natick, MA, USA) using custom written code as well as code imported from the HOSAtoolbox (Swami et al. 2003) for bispectral analysis. It is necessary to reiterate that the nonlinearity of a time-series is expressed by the phase correlation across different frequencies. We used the lowest order (third order) phase coupling, described by the bispectrum and first used in ocean waves by Hasselmann (1963), to analyze the hippocampal LFP, as we previously described in Sheremet et al. (2016). It is emphasized here as well as elsewhere (Pradhan et al. 2012; Van Milligen et al. 1995) that the bispectrum measures phase coupling, defined to occur when the sum of phases between two frequencies is equal to the value of a third frequency plus a constant. In order to associate our analysis with speed, the one-second of LFP for the bispectrum was stored with the mean velocity for the same temporal epoch. Based on mean velocities of every segment, we classified each LFP segment into 4 speed ranges: 0.001 to 5 cm/s; 5 to 15 cm/s; 15 to 35 cm/s; and > 35 cm/s. For statistical comparisons, average nonlinearity was calculated for the 5 to 15 cm/s speed bin andand the > 35 cm/s bin.

bioRxiv preprint doi: https://doi.org/10.1101/422246; this version posted September 19, 2018. The copyright holder for this preprint (which was not certified by peer review) is the author/funder, who has granted bioRxiv a license to display the preprint in perpetuity. It is made available under aCC-BY-NC-ND 4.0 International license.

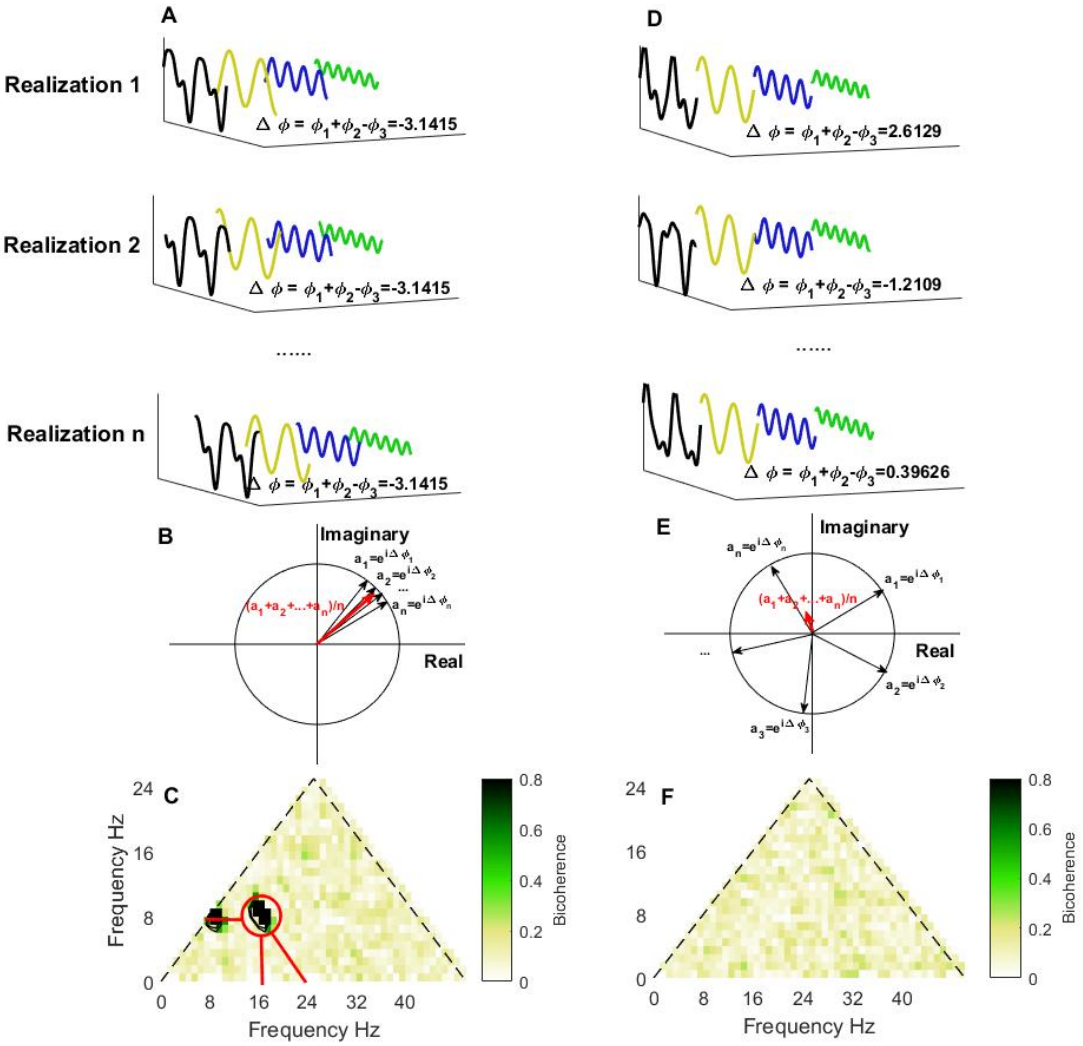

Figure 2: Bicoherence illustration. **A**, Time series with triad phase coupling (black line) resolved into Fourier series where the main components are three sinusoidal waves with frequencies: $f1 = 8$ Hz (yellow), $f2 = 16$ Hz (blue) and $f3 = f1 + f2 = 24$ Hz (green). The biphase of the three waves is defined as $\Delta\phi = \phi_{f_1} + \phi_{f_2} - \phi_{f_3}$. The biphase is almost constant over realizations. Averaging biphase vectors over realizations $\frac{\sum_{k=1}^{n} e^{i\Delta\phi_k}}{n} \approx e^{i\Delta\phi_k}$ gives a complex number which has the norm. close to 1 as shown in **B**. The frequency triad (f1; f2; f3) is corresponding to the significant region (marked with red circle) in bicoherence plot **C**. Figure **C** shows the modulus of the averaged biphase vectors $\left|\frac{\sum_{k=1}^{n} e^{i\Delta\phi_k}}{n}\right|$ for all the frequency triads. The contour lines in **C** outline the 99% significance level on zero bicoherence which is suggested by Elgar and Guza (1985) as $\sqrt{6/n}$. The marked significant region indicates the frequency of three waves: 8 Hz, 16 Hz and 24 Hz (indicated with red lines). The $y = x$ boundary of bicoherence plot **C** is imposed by the symmetry property of bicoherence; and the $x + y = 50$ boundary is imposed by the up limit of frequency range of interested ($fx + fy = 50\,Hz$). In **C**, there is another significant region (8 Hz, 8Hz & 16Hz) which implies this triad is also phase coupled. **D**, Time series without triad phase coupling (black line) and the Fourier series components with frequency $f1 = 8$ Hz(orange), $f2 = 16$ Hz (blue) and $f3 = 24$ Hz (green). The biphase $\Delta\phi$ distributes randomly, and the biphase vectors $e^{i\Delta\phi_k}$cancel each other when averaging over realizations as shown in **E**, which gives a bicoherence plot without any significant regions in **F**.

bioRxiv preprint doi: https://doi.org/10.1101/422246; this version posted September 19, 2018. The copyright holder for this preprint (which was not certified by peer review) is the author/funder, who has granted bioRxiv a license to display the preprint in perpetuity. It is made available under aCC-BY-NC-ND 4.0 International license.

Results:

For a preliminary measure of laminar differences of local field potential, we calculated the power spectral density in the CA1 oriens (Or.), stratum pyramidale (CA1.pyr), radiatum (CA1.rad), and lacunosum-moleculare (LM) as a function of speed (**Fig. 3**). Our observations of the power spectra can be characterized in general as having a power law $f^{-\alpha}$ structure. However, unlike previous reports, the spectral slope α is not constant throughout the entire frequency range. Instead, two or more domains with distinct slopes can be identified, most evident in the LM. Using preliminary analyses across layers of the power spectral density, cross-frequency phase-power coherence and bicoherence analyses, these domains formed rather well-defined frequency intervals that can be associated with theta (6-10 Hz) and its harmonics (16Hz, 24Hz, 32Hz, 40Hz and 48Hz; see nonlinear analysis below); gamma (broadly defined here as ~50-120 Hz similar to Bragin et al. 1995); and fast oscillations (> 120 Hz). Adjacent hippocampal layers also exhibited harmonics of theta, although not as prominent as the LM region. In agreement with previous results (Bragin et al. 1995), theta and gamma power are higher in the LM than the other CA1 layers.

In the 50-120 Hz frequency range, the distribution of power acquires the form of a front of constant slope shifting to the right, toward higher frequencies as running speed increases (inset in Figure **3**). This effect is observed across all layers. While the increase in theta power with velocity is in congruence with models by which theta is driven by an external input (Buzsaki 2002; Holsheimer et al. 1982), the shifting gamma front is indicative of a change in circuit dynamics. Specifically, previous work on central pattern generators suggest that high-frequency oscillations can increase as a function of

bioRxiv preprint doi: https://doi.org/10.1101/422246; this version posted September 19, 2018. The copyright holder for this preprint (which was not certified by peer review) is the author/funder, who has granted bioRxiv a license to display the preprint in perpetuity. It is made available under aCC-BY-NC-ND 4.0 International license.

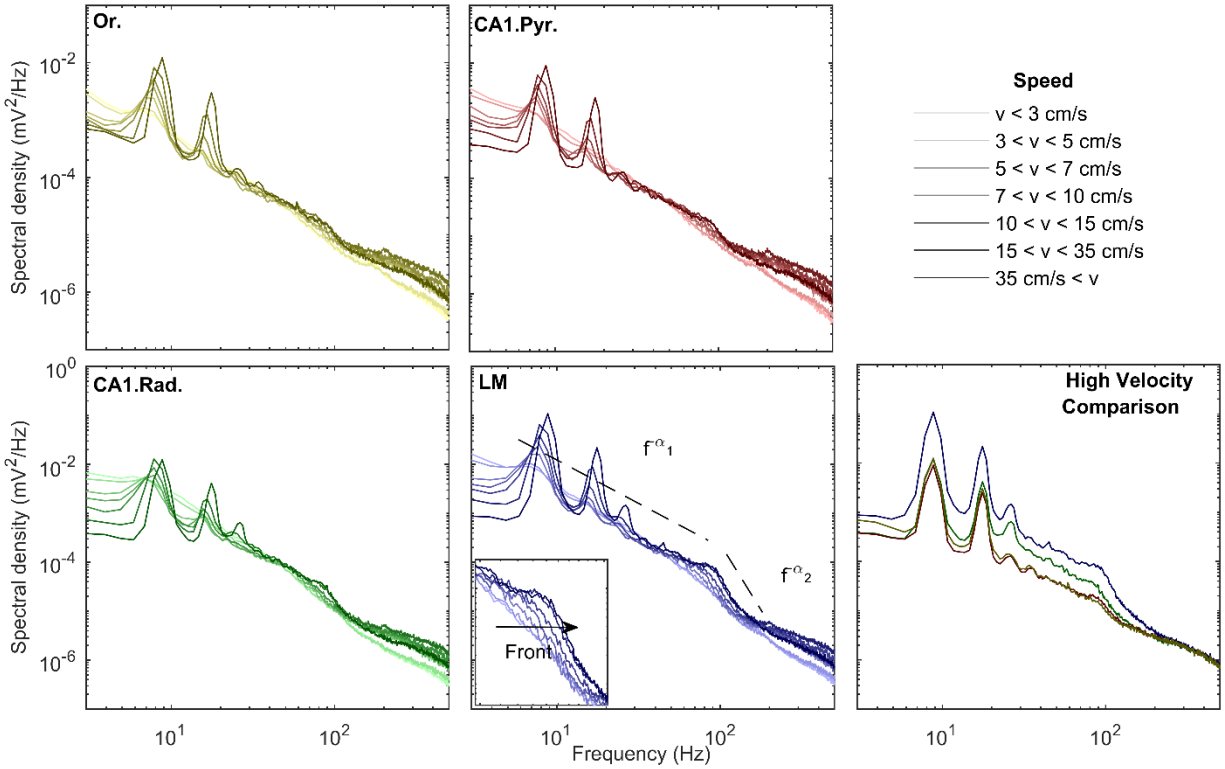

Figure 3. Changes in power spectral density as a function of velocity and CA1 layer (transition from lighter to darker hues indicate low to high velocities). Note that, across all layers, the increases in theta and theta harmonic with speed are associated with an increase in gamma power. Insets show details of the evolution of the gamma range (magnification of gray rectangle area). Spectral shapes in all layers follow a power laws of the type $f^{-\alpha}$. Remarkably, the LM layers exhibits different slopes between the frequency domains that encompass theta and its harmonics and the gamma range. This phenomenon becomes apparent in all regions when comparing all high velocity power spectra across layers (bottom right). Furthermore, as power increases in the gamma range, the spectrum preserves its slope and shifts to the right, creating the appearance of a moving front (inset of LM). Note that, in agreement with prior publications (Bragin et al., 1995), the CA1 oriens and pyramidal layer exhibit the least energetic gamma range of all the layers examined.

neural drive (Shik et al. 1969). To test this hypothesis relative to the hippocampus, we examined power- power correlations between the theta and gamma bands. If the gamma frequency component of the LFP is excited by the same input as theta, the two oscillatory frequencies should exhibit “power-power” correlations. Therefore, we calculated power for hippocampal theta (narrowly defined as 6-10Hz for this analysis) relative to gamma power (using a range from 50-120Hz) in 1-second windows. By correlating the power of the hippocampal theta rhythm against the power of the gamma within the same region, it is possible to determine whether a power-power relationship

bioRxiv preprint doi: https://doi.org/10.1101/422246; this version posted September 19, 2018. The copyright holder for this preprint (which was not certified by peer review) is the author/funder, who has granted bioRxiv a license to display the preprint in perpetuity. It is made available under aCC-BY-NC-ND 4.0 International license.

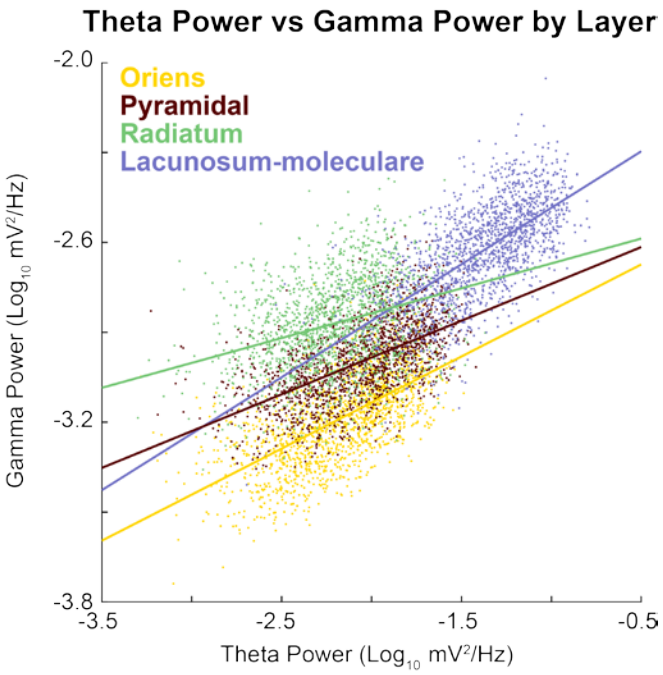

Slopes

Layer	530	538	539	544	695	Mean ± Std Dev.
o	0.17	0.15	0.02	0.15	0.21	0.14 ± 0.07
p	0.13	0.12	0.01	0.09	0.17	0.10 ± 0.06
r	0.23	0.19	0.10	0.35	0.29	0.23 ± 0.09
lm	0.18	0.20	0.13	0.29	0.16	0.19 ± 0.06

Intercept

Layer	530	538	539	544	695	Mean ± Std Dev.
o	-2.61	-2.56	-2.64	-2.28	-1.36	-2.29 ± 0.54
p	-2.77	-2.82	-2.93	-2.41	-1.79	-2.54 ± 0.46
r	-2.64	-2.56	-2.66	-2.12	-1.40	-2.27 ± 0.54
lm	-2.53	-2.43	-2.47	-2.12	-1.65	-2.24 ± 0.37

Correlation coefficient

Layer	530	538	539	544	695	Mean ± Std Dev.
o	0.38	0.35	0.06	0.34	0.41	0.31 ± 0.14
p	0.31	0.26	0.04	0.19	0.42	0.24 ± 0.14
r	0.57	0.44	0.21	0.70	0.61	0.51 ± 0.19
lm	0.41	0.45	0.31	0.60	0.43	0.44 ± 0.10

Figure 4. Correlation of theta power to gamma power. (**Left**) Scatter plot and least-squared regression lines for theta and gamma power across the layers of rat 695. Note that there is a clear positive trend across all layers, although strongest in the lacunosum-moleculare. (**Right**) Table containing the individual rat data (slope, intercept and correlation coefficient) by layer as well as averages.

exists (**Fig. 4**). Across lamina and rats there was a significant relationship between theta power and gamma power with, on average, 16% of the variance in gamma power being explained by theta power ($p = 0.04$). Interestingly, the correlation coefficients between theta and gamma power significantly differed between hippocampal lamina ($F_{[3,12]} = 10.21$, $p = 0.001$). In fact, the correlation between theta and gamma power was highest in the CA1.Rad ($r = 0.51$) and lowest in the CA1.Pyr ($r = 0.24$). Simple orthogonal contrasts comparing the CA1.Rad to the other CA1 lamina indicated that the theta-gamma power correlation was significantly greater in the CA1.Rad compared to the Or ($F_{[1,4]} = 19.74$, $p = 0.01$) and the CA1.Pyr ($F_{[1,4]} = 16.98$, $p = 0.02$). In contrast, the correlation between theta and gamma power was not significantly different between the CA1.Rad and LM ($F_{[1,4]} = 2.11$, $p = 0.22$). These data indicate that theta and gamma power are strongly correlated across all layers, and that this relationship is particularly

bioRxiv preprint doi: https://doi.org/10.1101/422246; this version posted September 19, 2018. The copyright holder for this preprint (which was not certified by peer review) is the author/funder, who has granted bioRxiv a license to display the preprint in perpetuity. It is made available under aCC-BY-NC-ND 4.0 International license.

344 evident in the CA1.Rad and LM.

345 The slope of the relationship between theta and gamma power provides
346 information regarding the rate at which activity transfers across frequency bands. The
347 slope was significantly different across hippocampal laminae ($F_{[3,12]} = 7.52$, $p = 0.004$).
348 The slope was greatest in the CA1.Rad (b = 0.23 where b stands for the slope) and
349 smallest in the CA1.Pyr (b = 0.11). Simple orthogonal contrasts comparing the CA1.Rad
350 to the other CA1 lamina indicated that the slope of the theta-gamma power relationship
351 was significantly greater in the CA1.Rad compared to the Or ($F_{[1,4]} = 10.64$, $p = 0.03$)
352 and CA1.Pyr ($F_{[1,4]} = 14.63$, $p = 0.02$). In contrast, the slope of the theta-gamma power
353 relationship was not significantly different between the CA1.Rad and LM ($F_{[1,4]} = 2.11$, p
354 $= 0.22$). This observation is not trivial as it runs counter to contemporary models in
355 which neural oscillations considered to be independent and multiplexed (Akam and
356 Kullmann 2014; McLelland and VanRullen 2016). Multiplexing implies that different
357 frequencies, supported by orthogonal populations of neurons (e.g., Gloveli et al. 2005),
358 can vary their activity independently of each other (which would be evident should theta-
359 to gamma-power exhibit little to no correlation). Rather, these observations indicate
360 that, across layers, gamma increases power in proportion to the amount of theta
361 activity, supporting the hypothesis that external neural drive (theta) provides the activity
362 that supports the amplitude of the gamma oscillation.

363 Although there was a significant, positive correlation in between theta and
364 gamma power and power increases with velocity, it may be argued that these results do
365 not fully encompass cross-frequency interactions, let alone demonstrate dependency.
366 Therefore, we investigated the average cross-frequency phase-power coherency

bioRxiv preprint doi: https://doi.org/10.1101/422246; this version posted September 19, 2018. The copyright holder for this preprint (which was not certified by peer review) is the author/funder, who has granted bioRxiv a license to display the preprint in perpetuity. It is made available under aCC-BY-NC-ND 4.0 International license.

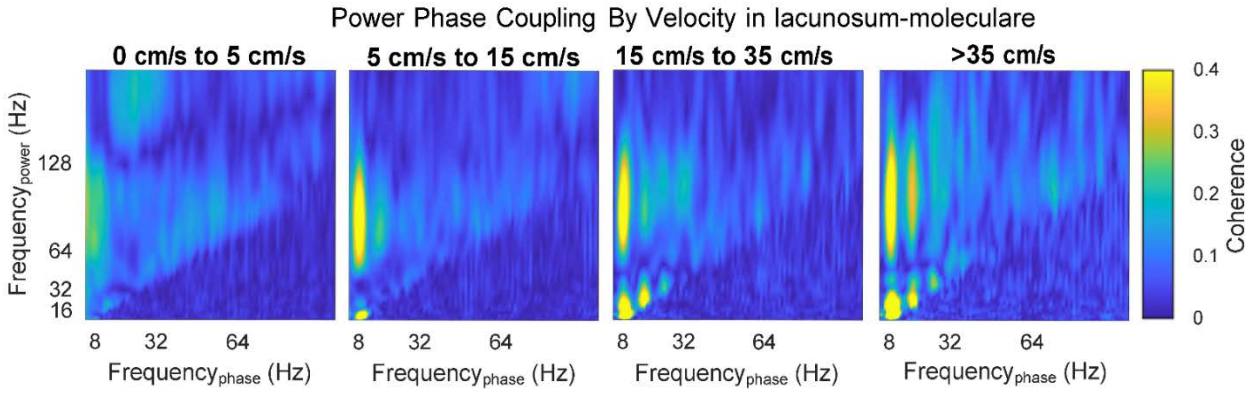

Figure 5: Example cross-frequency coherence between oscillatory power and oscillatory phase as a function of velocity for the lacunosum-moleculare. Note that, as velocity increases, there are low frequency interactions between theta and its harmonics (sub 40Hz). As harmonics by definition are integer, phase locked components to a fundamental oscillation, and the deformation of theta from sinusoid to sawtooth increases with velocity (Buzsáki et al. 1983; Sheremet et al. 2016; Terrazas et al. 2005), this effect is to be expected. Interestingly, there is a notable increase in the coupling between theta phase and gamma power – as well as theta harmonic phase and gamma power- with velocity.

(Colgin et al. 2009) as a function of velocity. Across layers, gamma power-theta phase coherence increased as a function of velocity (**Fig. 5**). As theta transitions from a sinusoidal oscillation to a "saw-tooth" shape with increasing velocity, higher-order harmonics are cast in the spectral decomposition (Buzsáki et al. 1983; Sheremet et al. 2016; Terrazas et al. 2005). Notably, phase-power coherence also increased between the harmonics of theta with velocity as well as between the phase of the 16Hz harmonic and the power of gamma. As the 16Hz is not an independent oscillation from theta, but simply an oscillatory deformation, the interaction between theta and gamma encompasses both the 8hz and 16Hz component. Therefore, in order to quantify the power-phase coherence increase with velocity, the average coherence was calculated for theta phase (8Hz)-gamma power and 16Hz harmonic phase-gamma power. Calculating the difference between the high velocity bin (>35 cm/s) and low (5-15 cm/s) revealed a consistent increase in gamma power and the phase of the theta complex (**Fig. 6**).

bioRxiv preprint doi: https://doi.org/10.1101/422246; this version posted September 19, 2018. The copyright holder for this preprint (which was not certified by peer review) is the author/funder, who has granted bioRxiv a license to display the preprint in perpetuity. It is made available under aCC-BY-NC-ND 4.0 International license.

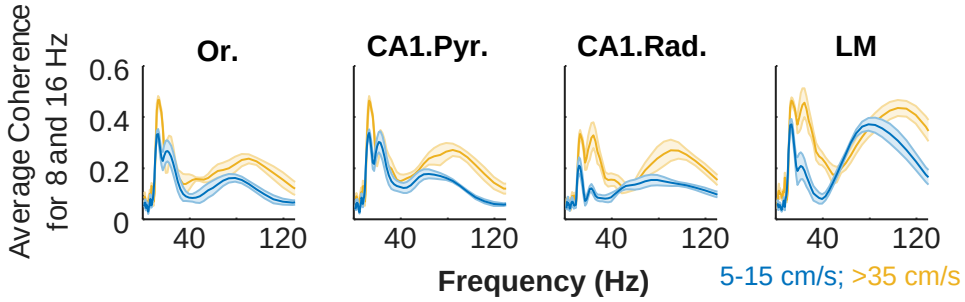

Figure 6: Average cross-frequency coherence for theta and the 16Hz theta harmonic phase. By averaging the coherence for these specific phases, there is a considerable change in cross-frequency coherence with velocity. Each subplot shows the individual layers of the hippocampus with yellow as the high, >35 cm/s velocity bin and blue as the 5-15 cm/s bin (Or., oriens; CA1.Pyr, pyramidal layer; CA1.Rad., radiatum; LM, lacunosum-moleculare). The shaded errorbars depict the mean and standard error of the mean (n = 5). Note that in the gamma range, greater than 50Hz, there is both an increase in coherence that is associated with a shift of the maximum value to higher frequencies (see Fig. 3). The changes in the low value frequencies, less than 40Hz, are attributed to the higher order harmonics of theta (e.g., 24 and 32Hz; see bicoherence analysis below).

As the power and phase of theta both exhibited a strong effect on gamma power, which increases in magnitude as a function of velocity, it suggests that the two oscillations are in fact part of a unitary process. Rather than the hippocampal spectra being akin to decomposition of an orchestra, with different frequencies attributable to specific, non-interacting instruments, it appears that there is a direct dependency that is analogous to ocean waves in which waves of different length form a cooperative system in which they sustain each other (e.g., Longuet-Higgins 1992). Stated simply, the LFP of the hippocampus reflects a multiscale phenomenon, driven by a flow of energy from low to high frequencies across the spectrum (Buzsaki 2006). In this energy cascade framework, it would suggest that theta-gamma interactions are dependent, with the degree of phase-phase interactions directly proportional to energy/activity in the network. However, the analytical approaches of cross-frequency phase-phase coupling

bioRxiv preprint doi: https://doi.org/10.1101/422246; this version posted September 19, 2018. The copyright holder for this preprint (which was not certified by peer review) is the author/funder, who has granted bioRxiv a license to display the preprint in perpetuity. It is made available under aCC-BY-NC-ND 4.0 International license.

have been recently called into question, due to distortions in filtering and not accounting for harmonic (Scheffer-Teixeira and Tort 2016). As described in the methods, bicoherence has been used extensively to quantify the degree of cross-frequency phase-phase coupling in the LFP, investigating the relationship between a wide band of frequencies and can be implemented to directly identify harmonics. Therefore, we investigated the degree of phase coupling within hippocampal layers as a function of velocity using bicoherence analyses.

As previously reported, bispectral estimates of theta and the respective harmonics show significant variability with rat running speed, with limited significant interactions at velocity < 10cm/s (**Fig. 7**). In contrast, at higher running speeds (i.e., velocity > 40 cm/s, **Fig. 8**) the bispectral map shows a rich phase-coupling structure. In agreement with the observations of power spectral density evolution (Fig. **3**), strong phase coupling develops between theta (theta frequency $f_\theta \approx 8$ Hz) and its harmonics (f_θ , with $n = 2,3,4, \ldots$), with peaks detectable at frequencies below ~50 Hz, at various strengths, across all layers. It is worth emphasizing that the development of theta harmonics strongly coupled to theta indicates a nonlinear deformation of the theta rhythm toward positive skewness and asymmetry and should not be attributed to the generation of additional, statistically independent rhythms. Rather, the saw-tooth shape of theta causes a 48 Hz frequency to register in the oscillatory decomposition of LFP.

Furthermore, the increase of theta power and nonlinearity is accompanied by the development of significant phase coupling between theta and gamma oscillations, related to interaction between rhythms, rather than to nonlinear shape deformation. Theta-gamma coupling covers the entire gamma frequency band (the wide bands

bioRxiv preprint doi: https://doi.org/10.1101/422246; this version posted September 19, 2018. The copyright holder for this preprint (which was not certified by peer review) is the author/funder, who has granted bioRxiv a license to display the preprint in perpetuity. It is made available under aCC-BY-NC-ND 4.0 International license.

located at $50\ \mathrm{Hz} < f_1 < 100$ Hz and $f_2 \approx 8$ Hz). The effect is again strongest in the LM, where interacting triads of the form (f_γ , f_θ , $f_\gamma + f_\theta$) , and (f_γ , $2f_\theta$, $f_\gamma + 2f$) are obvious, where f is a frequency in the gamma band. As the location and magnitude of the bicoherence peaks identify and measure the intensity of cross-phase interactions, the strength of the nonlinear coupling can be quantified by integrating the bicoherence over the region of interest (**Fig. 9**). In agreement with the results presented in Sheremet et al. (2016), the nonlinearity was significantly greater at faster running speeds ($F_{[1,16]}$ =31.09, p = 0.001; repeated-measures). Moreover, nonlinearity also varied significantly as a function of CA1 laminae ($F_{[3,16]}$ =11.96, p = 0.001), with the LM being significantly more nonlinear compared to the other 3 laminae (p < 0.002 for all comparisons, Tukey HSD). The bicoherence values across the Or, CA1.Pyr and CA1.Rad, however, were not significantly different (p > 0.76 for all comparisons). The difference in nonlinearity between low and high velocities did not significantly interact with layer ($F_{[3,16]}$ = 0.21, p = 0.89), indicating that the impact of faster speeds on nonlinearity was similar across all CA1 laminae.

When the quantification of nonlinearity was restricted to the theta (6-32 Hz) and gamma (50-120 Hz) frequency ranges (Fig 7), there was also a strong effect of velocity on nonlinearity ($F_{[1,16]}$ =38.53, p = 0.0001; repeated measures). Within the theta and gamma frequency ranges there was also a significant effect of layer on nonlinearity ($F_{[3,16]}$ =19.87, p = 0.001), that did not significantly interact with velocity ($F_{[3,16]}$ = 0.48, p = 0.70). Interestingly, the theta-gamma bicoherence values in the LM were significantly greater than the other 3 laminae (p < 0.001 for all comparisons; Tukey HSD). The

bioRxiv preprint doi: https://doi.org/10.1101/422246; this version posted September 19, 2018. The copyright holder for this preprint (which was not certified by peer review) is the author/funder, who has granted bioRxiv a license to display the preprint in perpetuity. It is made available under aCC-BY-NC-ND 4.0 International license.

nonlinearity between the Or, CA1.Py and CA1.Rad was not significantly different, however ($p > 0.32$ for all comparisons; Tukey HSD).

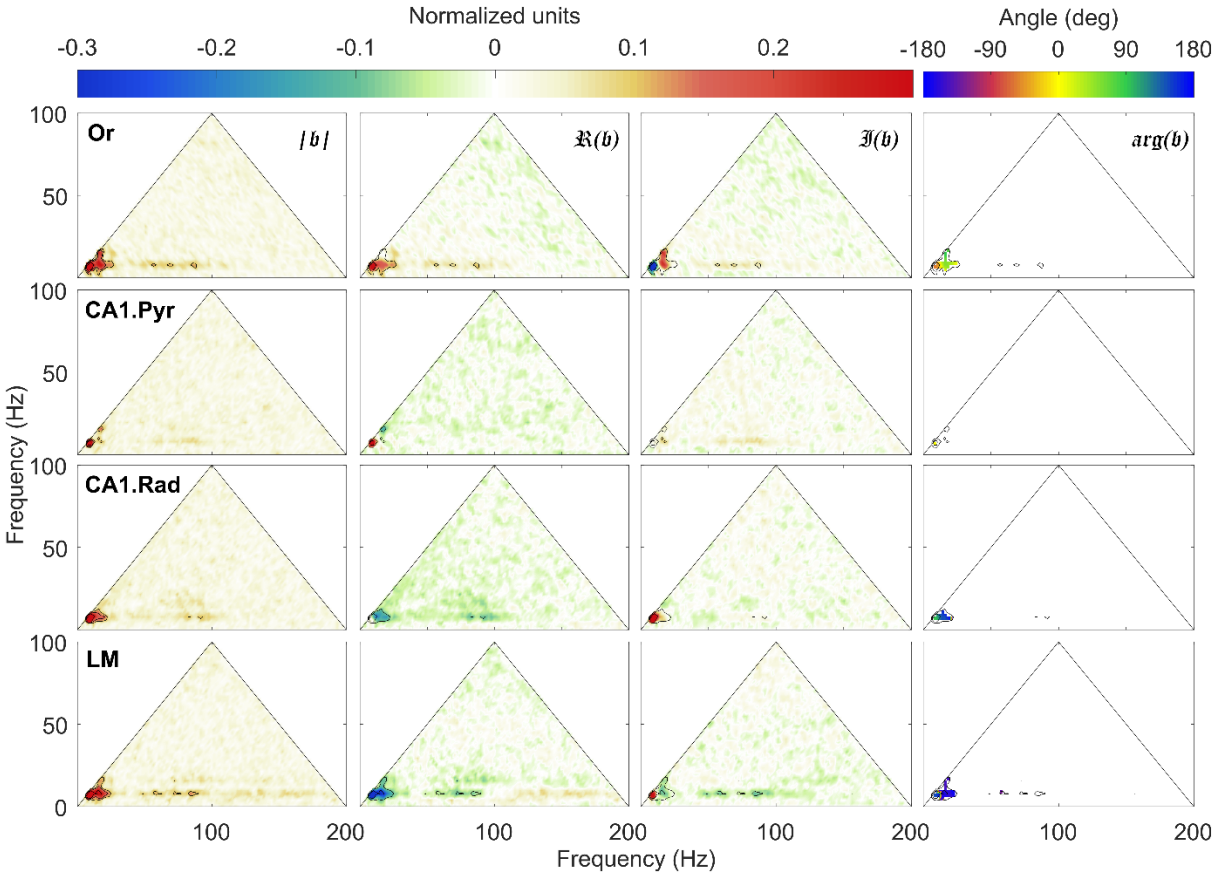

Figure 7: Normalized bispectrum (equation 11) at low speeds (v < 10 cm/s). An in-depth explanation of the bicoherence plot can be found in Sheremet et al. (2016) Briefly, the triangular region represents the area containing non-redundant information for the discrete Fourier transform. Columns (left to right) show the bicoherence |𝔟|, the real $\Re(\mathfrak{b})$ and imaginary $\Im(\mathfrak{b})$ parts of the normalized bispectrum $\mathfrak{b}$, and the biphase arg(𝔟). The first three can be interpreted as nonlinearity strength, and measures of the contribution of different triads to the skewness and asymmetry of the LFP. Peak in the bispectral estimate represents a phase-coupled triplet ($f_1, f_2, f_1 + f_2$), where f_j, j = 1,2 are frequency bands in the Fourier representation. The observations in each row correspond to a given hippocampal layer. For each layer, black contours mark the significant bicoherence value of 0.1 (with 300 DOF, zero-mean bicoherence is <0.1 at 95% confidence level.

bioRxiv preprint doi: https://doi.org/10.1101/422246; this version posted September 19, 2018. The copyright holder for this preprint (which was not certified by peer review) is the author/funder, who has granted bioRxiv a license to display the preprint in perpetuity. It is made available under aCC-BY-NC-ND 4.0 International license.

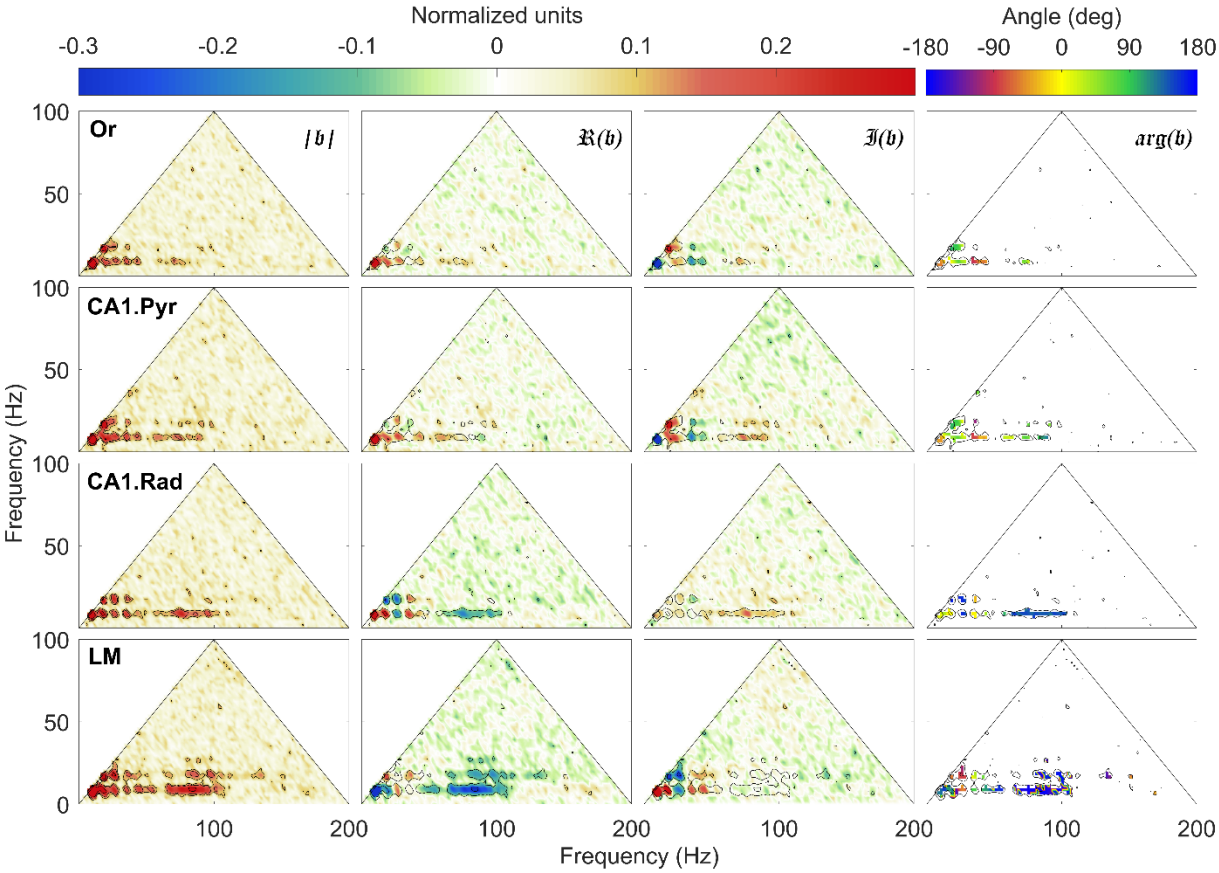

Figure 8. Normalized bispectrum at high speeds (v > 35 cm/s). Same organization as in figure 5. Note the development of multiple regions of high bicoherence |b|, notably: 1) t theta (theta frequency $f_\theta \approx 8$ Hz) and its harmonics (nf_θ , with $n = 2,3,4, \ldots$), with peaks detectable up to 48Hz across all layers, and 2) theta and a wide gamma band spanning approximately the interval between 60 Hz to 100 Hz. The LM exhibits the richest nonlinear structures of the four layers examined with gamma coupling to the first harmonic of theta.

bioRxiv preprint doi: https://doi.org/10.1101/422246; this version posted September 19, 2018. The copyright holder for this preprint (which was not certified by peer review) is the author/funder, who has granted bioRxiv a license to display the preprint in perpetuity. It is made available under aCC-BY-NC-ND 4.0 International license.

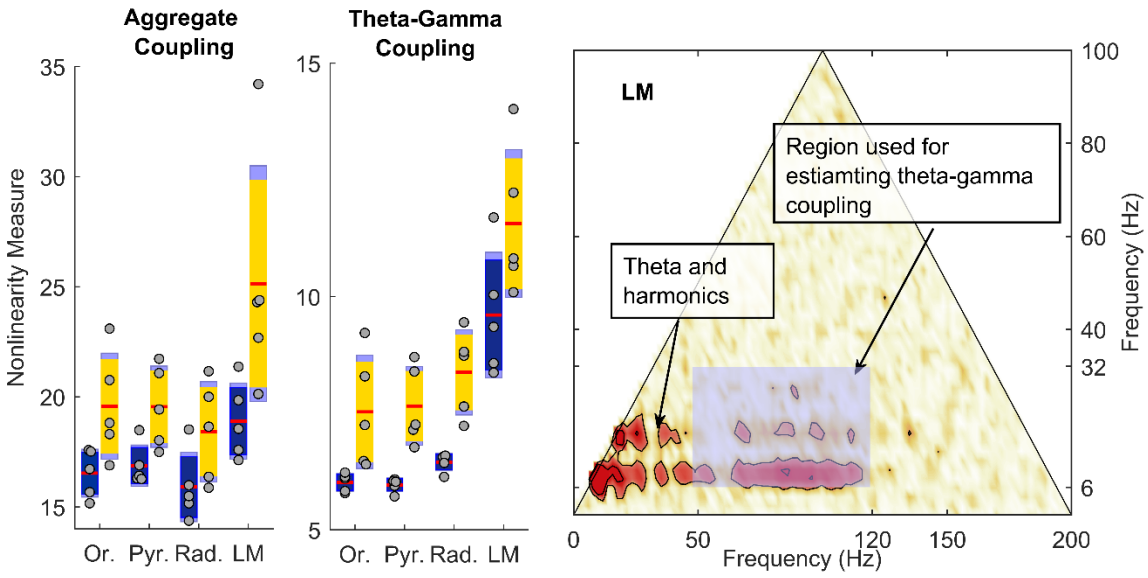

Figure 9. Estimate of nonlinear cross-frequency phase coupling. Left: Total overall strength of nonlinearity, estimated by summing the bicoherence over its entire definition domain. Estimates are shown for 5-15cm/s speed bin (blue) of >35cm/s speed bin (yellow). Middle: Strength of nonlinear coupling between theta (and hamonics) and gamma rhythms estimated by summing the bicoherence values in the shaded rectangle of right panel. The LM exhibits a significant larger coupling strength compared with the other layers. Both total and strictly theta-gamma coupling strength show significant variability as a function of rat speed and hippocampal layer. Note that the y-axis differs between nonlinearity measures in order to optimize for display of the theta-gamma-gamma nonlinearity. Red is the mean, solid dark blue or yellow is 1.96 of the standard error of the mean (S.E.M.) and light blue denotes the boundaries of 1 standard deviation. Right: Region used for estimating the strength of theta-gamma coupling is a rectangle covering the intervals [6 Hz, 32 Hz] for theta and [50 Hz, 120 Hz] for gamma.

Discussion:

The current paper reports the novel finding of power-power, phase-power, and phase-phase coupling between theta and gamma oscillations that is dependent on velocity, which varies in a layer dependent manner. Macroscopically, bouts of input at theta frequency provide the excitation/inhibition to organize synaptic activity rhythmically. Neurons within the entorhinal-hippocampal circuit are tuned to resonate at theta frequencies, evident in the ability of the hippocampus to locally generate theta when provided sufficient input (Bland et al. 1988; Fraser and MacVicar 1991; Kamondi et al. 1998; Kocsis et al. 1999; Konopacki et al. 1987). Therefore, when strongly driven, local

bioRxiv preprint doi: https://doi.org/10.1101/422246; this version posted September 19, 2018. The copyright holder for this preprint (which was not certified by peer review) is the author/funder, who has granted bioRxiv a license to display the preprint in perpetuity. It is made available under aCC-BY-NC-ND 4.0 International license.

circuits find a temporally stable interaction. This drive, in turn, activates small circuits, which – when "kicked hard"- provide a mechanism for endogenous timing. For example, this theta paced drive could conceivably cause basket cells to fire gamma frequency bursts at theta frequency (Bragin et al. 1995; Ylinen et al. 1995b). The consequence of this organization is that neuronal activity of both pyramidal cells and interneurons are organized to both the relatively slow theta oscillation and the faster gamma oscillation (Buzsáki and Chrobak 1995).

Increasing the total amount of activity into a network will have multiple consequences including more coincident synaptic events (reflected as increases in local field potential power). There is a dramatic increase in firing rates across hippocampal neurons with velocity (Hirase et al. 1999; Maurer et al. 2005; McNaughton et al. 1983). Moreover, running speed alters hippocampal sequence compression of place cell spikes (Maurer et al. 2012). Because the single units change their dynamics, and the LFP is generated by membrane events, it stands to reason that there must be associated changes in LFP power and gamma frequency (Ahmed and Mehta 2012; Chen et al. 2011; Kemere et al. 2013; Zheng et al. 2015). It is worth noting that there is a low fraction of observed gamma locking between CA3 or entorhinal LFP and CA1 pyramidal neurons (Schomburg et al. 2014). These observations support the idea that gamma can provide a measure of upstream temporal dynamics but fails to entrain the individual units (Buzsáki and Schomburg 2015). Rather, as the distal dendrites operate as a low-pass filter (Golding et al. 2005), theta-gamma paced synaptic input in the lacunosum-moleculare or radiatum are reverted to just theta at the soma (Vaidya and Johnston 2013). Nevertheless, the lacunosum-moleculare exhibited the highest theta-gamma

bioRxiv preprint doi: https://doi.org/10.1101/422246; this version posted September 19, 2018. The copyright holder for this preprint (which was not certified by peer review) is the author/funder, who has granted bioRxiv a license to display the preprint in perpetuity. It is made available under aCC-BY-NC-ND 4.0 International license.

coupling as a function of velocity suggesting that theta-modulated gamma inputs are conveyed from the entorhinal cortex (Fernández-Ruiz et al. 2017), which exhibits a high amount of sensitivity to path-integration and self-motion (Kropff et al. 2015; Moser and Moser 2008; Sargolini et al. 2006).

The interplay between theta and gamma rhythms as a function of velocity is not to suggest that theta is a required prerequisite for gamma. There are two considerations with respect to this point. First, the power spectra density of the local field potential demonstrates and $\sim\frac{1}{f^{\alpha}}$ slope, indicating that any frequency has the potential of being isolated. Power will exist across all frequencies, with low frequencies exhibiting the highest amplitude. Therefore, while there may not be a large peak in theta power, there still may be enough activity in the network that leads to local circuit entrainment at gamma frequency. Experimentally, this has been observed in situations in which severing the fimbria fornix or lesioning the entorhinal cortex severely diminished theta power, but yielded increases in gamma power (Bragin et al. 1995; Buzsáki et al. 1987). This highlights the second consideration, that it is the characteristics of neurons and the local network that defines the ability to capture the incoming activity. In the absence of entorhinal input, it is tenable that the network undergoes reorganization to compensate for the loss of input. This compensation results in an easier entrainment of local circuits (gamma) that occurs with weak, low frequency input across the population. Other aspects theoretically modulate the ability of local circuits to capture the global input including age-related synaptic changes and pharmacological manipulation.

The current manuscript links prior findings of theta-gamma interaction in the service of

bioRxiv preprint doi: https://doi.org/10.1101/422246; this version posted September 19, 2018. The copyright holder for this preprint (which was not certified by peer review) is the author/funder, who has granted bioRxiv a license to display the preprint in perpetuity. It is made available under aCC-BY-NC-ND 4.0 International license.

cognition (e.g., Jensen and Colgin 2007; Lisman and Jensen 2013; Montgomery et al. 2008; Tort et al. 2009; Tort et al. 2008) to other studies that have observed layer dependent theta-gamma effects during exploration (Belluscio et al. 2012; Lasztóczi and Klausberger 2016; or using datasets with and with out a mneumonic requirement Schomburg et al. 2014). The current data, however, point to a new perspective. In opposition to the idea that gamma and theta are driven by minimally overlapping mechanisms that couple under certain behavior conditions, we propose that coupling is enhanced in situations in which there is increased input into the network. Under increased input into the network, which occurs at faster running speeds or instances of high cognitive load, theta-gamma coupling could be utilized by local circuits to support higher-cognitive processes. For example, over the course of learning, theta paced inputs may result in higher power gamma oscillations through experience-dependent plasticity. In this manner, in the awake-behaving animal, theta and gamma are interdependent, coupled by the cascade of energy across spatial and temporal (frequency) scales (Buzsaki, 2006).

This perspective, however, runs counter to the recent theory of oscillatory multiplexing in the brain, where individual frequencies carry different components of information (e.g., Akam and Kullmann 2014; McLelland and VanRullen 2016). For example, it has been suggested that communication across brain regions may occur in a frequency specific manner and aspects of cognition can be determined through calculating cross-regional coherence, with different bands conveying different psychological components (Knight and Eichenbaum 2013; Siegel et al. 2012; Watrous et al. 2013). Moreover, neuron populations with heterogeneity in the preferred phase coupling frequency would

bioRxiv preprint doi: https://doi.org/10.1101/422246; this version posted September 19, 2018. The copyright holder for this preprint (which was not certified by peer review) is the author/funder, who has granted bioRxiv a license to display the preprint in perpetuity. It is made available under aCC-BY-NC-ND 4.0 International license.

551 theoretically provide a mechanism to communicate and organize the spike firing times
552 of multiple, distant cell assemblies in a frequency specific manner (Canolty et al. 2010).
553 However, this entrainment by oscillatory coherence may be an over-simplification. For
554 example, the dendrites of hippocampal pyramidal neurons operate as a low pass filter
555 (Golding et al. 2005; Vaidya and Johnston 2013), which would suggest that gamma
556 frequency activity within the lacunosum-moleculare (the afferent input layer of the
557 entorhinal cortex) has little consequence on the gamma frequency activity within the
558 pyramidal layer. This is evident in the relatively low coherence of gamma frequences
559 between the medial entorhinal cortex and pyramidal layer when compared to theta
560 coherence between the same two regions (~0.3 and ~0.85 respectively, Colgin et al.
561 2009). Therefore, rather than coherence, external inputs entrained at gamma may
562 instead provide the necessary input to coordinate the phase of theta within a network
563 (Lopez-Madrona et al. 2018). Tersely, entorhinal input at gamma frequency supports
564 theta paced dynamics, and the energy cascade begins again. This line of reasoning
565 raises the critical consideration that marginal coherence values (stated differently,
566 incoherence) may not be biologically meaningful and coupling measures may risk
567 interchanging correlation for consequence. Rather, it may not be the frequency of
568 communication that is important, but the total amount of activity into the network.

569 The cascade theory suggests that it is improvident to assign a particular psychological
570 process to a specific frequency for the reason that, in the awake behaving animal, the
571 gamma rhythm is shaped by the activity in the theta band making the two oscillations
572 interdependent. Indisputably, the iterative processing and nonlinearity of neural circuits
573 make it implausible to assign a cause and effect relationship between a cognitive

bioRxiv preprint doi: https://doi.org/10.1101/422246; this version posted September 19, 2018. The copyright holder for this preprint (which was not certified by peer review) is the author/funder, who has granted bioRxiv a license to display the preprint in perpetuity. It is made available under aCC-BY-NC-ND 4.0 International license.

process and a narrow oscillatory band. The local field potential, however, is diagnostic of the underlying interactions, providing information to the experimenter with respect to *how the network is predisposed to organize*. In fact, synaptic events – contributing the ionic flux that shapes the LFP – have no knowledge with respect to whether they are supporting "gamma" or "theta." Parsing oscillatory frequencies to specific biophysical mechanisms, circuits or behavioral correlations for the purposes of higher-cognition loses relevance if the nervous system does not make the distinction (unless it is done for diagnostic purposes as described in the condition).

While assigning certain frequency oscillations may be gratifying to the experimentalist, Fourier decomposition is an analytical tool, far removed from synaptic or circuit dynamics. For example, often it is tempting to construct a power spectra and ask a question regarding deviations away from the $\frac{1}{f^{\alpha}}$ slope (e.g., after whitening). In the current manuscript, we demonstrate that the spectral slope α is not constant throughout the entire frequency range, demonstrating a methodological flaw to standard whitening techniques. Moreover, our spectral decomposition revealed 16, 24, 32, 40 Hz and higher harmonics of theta (Sheremet et al. 2016). While the decomposition "uncovers" these oscillations, the harmonics are the consequence of a single aggregate process in which theta changes from a sinusoid into a sawtooth with high asymmetry and skewness. Furthermore, there is an associated loss of power between ~1-6 Hz as running speed increases (Fig. 3). Interestingly, the loss of lower frequency power along with the development of the harmonics suggests that, as the amount of input increases, the initial effect will not necessarily be the entrainment of local circuits at gamma frequency, but increasing the network activity in the theta band This hypothesis is

bioRxiv preprint doi: https://doi.org/10.1101/422246; this version posted September 19, 2018. The copyright holder for this preprint (which was not certified by peer review) is the author/funder, who has granted bioRxiv a license to display the preprint in perpetuity. It is made available under aCC-BY-NC-ND 4.0 International license.

supported by the observation of inhibition dependent theta resonance (Stark et al. 2013). When there is little to no input, interneurons that resonant at theta frequency will express incoherent entrainment between 1-6 Hz. As input increases, these neuron begin to resonate, with power redistributing into theta. Finally, as hippocampal activity increases with velocity, the oscillatory energy begins to extend beyond the theta resonance and begins to entrain local circuits at gamma frequency.

This theory of energy cascade is not novel. In fact, it shares similarity with the concepts of self-organized criticality (Bak et al. 1987). Self-organized criticality was broadly used to describe any system in which there is an inverse correlation between oscillatory power and oscillatory frequency. This concept later found an analogous home in neuroscience, describing both the shape of the power spectra as well as neuronal avalanches (Beggs and Plenz 2003; Beggs and Timme 2012; Plenz and Thiagarajan 2007). With these insights, it is possible to consider the mechanisms by which the brain gives rise to cognition by relating activity through neural circuits.

bioRxiv preprint doi: https://doi.org/10.1101/422246; this version posted September 19, 2018. The copyright holder for this preprint (which was not certified by peer review) is the author/funder, who has granted bioRxiv a license to display the preprint in perpetuity. It is made available under aCC-BY-NC-ND 4.0 International license.

References

Ahmed OJ, and Mehta MR. Running speed alters the frequency of hippocampal gamma oscillations. *J Neurosci* 32: 7373-7383, 2012.

Akam T, and Kullmann DM. Oscillatory multiplexing of population codes for selective communication in the mammalian brain. *Nat Rev Neurosci* 15: 111-122, 2014.

Bak P, Tang C, and Wiesenfeld K. Self-organized criticality: An explanation of the 1/f noise. *Phys Rev Lett* 59: 381-384, 1987.

Barnett TP, Johnson LC, Naitoh P, Hicks N, and Nute C. Bispectrum analysis of electroencephalogram signals during waking and sleeping. *Science* 172: 401-402, 1971.

Beggs JM, and Plenz D. Neuronal avalanches in neocortical circuits. *J Neurosci* 23: 11167-11177, 2003.

Beggs JM, and Timme N. Being critical of criticality in the brain. *Front Physiol* 3: 163, 2012.

Belluscio MA, Mizuseki K, Schmidt R, Kempter R, and Buzsáki G. Cross-frequency phase-phase coupling between θ and γ oscillations in the hippocampus. *J Neurosci* 32: 423-435, 2012.

Bieri KW, Bobbitt KN, and Colgin LL. Slow and fast γ rhythms coordinate different spatial coding modes in hippocampal place cells. *Neuron* 82: 670-681, 2014.

Bland BH, Colom LV, Konopacki J, and Roth SH. Intracellular records of carbachol-induced theta rhythm in hippocampal slices. *Brain Res* 447: 364-368, 1988.

Bragin A, Jandó G, Nádasdy Z, Hetke J, Wise K, and Buzsáki G. Gamma (40-100 Hz) oscillation in the hippocampus of the behaving rat. *J Neurosci* 15: 47-60, 1995.

Bullock TH, Achimowicz JZ, Duckrow RB, Spencer SS, and Iragui-Madoz VJ. Bicoherence of intracranial EEG in sleep, wakefulness and seizures. *Electroencephalogr Clin Neurophysiol* 103: 661-678, 1997.

Buzsaki G. *Rhythms of the Brain*. Oxford University Press, 2006.

Buzsaki G. Theta oscillations in the hippocampus. *Neuron* 33: 325-340, 2002.

Buzsáki G. Theta rhythm of navigation: link between path integration and landmark navigation, episodic and semantic memory. *Hippocampus* 15: 827-840, 2005.

Buzsáki G, and Chrobak JJ. Temporal structure in spatially organized neuronal ensembles: a role for interneuronal networks. *Curr Opin Neurobiol* 5: 504-510, 1995.

Buzsáki G, Czopf J, Kondákor I, and Kellényi L. Laminar distribution of hippocampal rhythmic slow activity (RSA) in the behaving rat: current-source density analysis, effects of urethane and atropine. *Brain Res* 365: 125-137, 1986.

Buzsáki G, and Draguhn A. Neuronal oscillations in cortical networks. *Science* 304: 1926-1929, 2004.

Buzsáki G, Gage FH, Czopf J, and Björklund A. Restoration of rhythmic slow activity (theta) in the subcortically denervated hippocampus by fetal CNS transplants. *Brain Res* 400: 334-347, 1987.

Buzsáki G, Geisler C, Henze DA, and Wang XJ. Interneuron Diversity series: Circuit complexity and axon wiring economy of cortical interneurons. *Trends Neurosci* 27: 186-193, 2004.

Buzsáki G, Leung LW, and Vanderwolf CH. Cellular bases of hippocampal EEG in the behaving rat. *Brain Res* 287: 139-171, 1983.

Buzsáki G, and Schomburg EW. What does gamma coherence tell us about inter-regional neural communication? *Nat Neurosci* 18: 484-489, 2015.

Buzsáki G, and Wang XJ. Mechanisms of gamma oscillations. *Annu Rev Neurosci* 35: 203-225, 2012.

Canolty RT, Ganguly K, Kennerley SW, Cadieu CF, Koepsell K, Wallis JD, and Carmena JM. Oscillatory phase coupling coordinates anatomically dispersed functional cell assemblies. *Proc Natl Acad Sci U S A* 107: 17356-17361, 2010.

Chen Z, Resnik E, McFarland JM, Sakmann B, and Mehta MR. Speed controls the amplitude and timing of the hippocampal gamma rhythm. *PLoS One* 6: e21408, 2011.

Chrobak JJ, and Buzsáki G. Gamma oscillations in the entorhinal cortex of the freely behaving rat. *J Neurosci* 18: 388-398, 1998.

Clayton JA. Studying both sexes: a guiding principle for biomedicine. *FASEB J* 30: 519-524, 2016.

bioRxiv preprint doi: https://doi.org/10.1101/422246; this version posted September 19, 2018. The copyright holder for this preprint (which was not certified by peer review) is the author/funder, who has granted bioRxiv a license to display the preprint in perpetuity. It is made available under aCC-BY-NC-ND 4.0 International license.

Colgin LL, Denninger T, Fyhn M, Hafting T, Bonnevie T, Jensen O, Moser MB, and Moser EI. Frequency of gamma oscillations routes flow of information in the hippocampus. *Nature* 462: 353-357, 2009.

Dragoi G, and Buzsáki G. Temporal encoding of place sequences by hippocampal cell assemblies. *Neuron* 50: 145-157, 2006.

Elgar S, and Guza R. Observations of bispectra of shoaling surface gravity waves. *Journal of Fluid Mechanics* 161: 425-448, 1985.

Fernández-Ruiz A, Oliva A, Nagy GA, Maurer AP, Berényi A, and Buzsáki G. Entorhinal-CA3 Dual-Input Control of Spike Timing in the Hippocampus by Theta-Gamma Coupling. *Neuron* 93: 1213-1226.e1215, 2017.

Fraser DD, and MacVicar BA. Low-threshold transient calcium current in rat hippocampal lacunosum-moleculare interneurons: kinetics and modulation by neurotransmitters. *J Neurosci* 11: 2812-2820, 1991.

Freund TF, and Buzsáki G. Interneurons of the hippocampus. *Hippocampus* 6: 347-470, 1996.

Gloveli T, Dugladze T, Rotstein HG, Traub RD, Monyer H, Heinemann U, Whittington MA, and Kopell NJ. Orthogonal arrangement of rhythm-generating microcircuits in the hippocampus. *Proc Natl Acad Sci U S A* 102: 13295-13300, 2005.

Golding NL, Mickus TJ, Katz Y, Kath WL, and Spruston N. Factors mediating powerful voltage attenuation along CA1 pyramidal neuron dendrites. *J Physiol* 568: 69-82, 2005.

GREEN JD, and ARDUINI AA. Hippocampal electrical activity in arousal. *J Neurophysiol* 17: 533-557, 1954.

Hagihira S, Takashina M, Mori T, Mashimo T, and Yoshiya I. Practical issues in bispectral analysis of electroencephalographic signals. *Anesthesia & Analgesia* 93: 966-970, 2001.

Harris B. *Spectral analysis of time series*. John Wiley & Sons, 1967.

Hasselmann K, Munk W, and MacDonald G. Bispectrum of ocean waves. In: *Proc Symp on Time Series Analysis*, edited by Rosenblatt M. New York: Wiley, 1963, p. 125-139.

Hirase H, Czurkó A, Csicsvari J, and Buzsáki G. Firing rate and theta-phase coding by hippocampal pyramidal neurons during 'space clamping'. *Eur J Neurosci* 11: 4373-4380, 1999.

Hjorth-Simonsen A. Some intrinsic connections of the hippocampus in the rat: an experimental analysis. *J Comp Neurol* 147: 145-161, 1973.

Holsheimer J, Boer J, Lopes da Silva FH, and van Rotterdam A. The double dipole model of theta rhythm generation: simulation of laminar field potential profiles in dorsal hippocampus of the rat. *Brain Res* 235: 31-50, 1982.

Ishizuka N, Weber J, and Amaral DG. Organization of intrahippocampal projections originating from CA3 pyramidal cells in the rat. *J Comp Neurol* 295: 580-623, 1990.

Jensen O, and Colgin LL. Cross-frequency coupling between neuronal oscillations. *Trends Cogn Sci* 11: 267-269, 2007.

Jung R, and Kornmüller A. Eine Methodik der Ableitung Iokalisierter Potentialschwankungen aus subcorticalen Hirngebieten. *European Archives of Psychiatry and Clinical Neuroscience* 109: 1-30, 1938.

Kamondi A, Acsády L, Wang XJ, and Buzsáki G. Theta oscillations in somata and dendrites of hippocampal pyramidal cells in vivo: activity-dependent phase-precession of action potentials. *Hippocampus* 8: 244-261, 1998.

Kemere C, Carr MF, Karlsson MP, and Frank LM. Rapid and continuous modulation of hippocampal network state during exploration of new places. *PLoS One* 8: e73114, 2013.

Kim Y, Beall J, Powers E, and Miksad R. Bispectrum and nonlinear wave coupling. *The Physics of Fluids* 23: 258-263, 1980.

Kim YC, and Powers EJ. Digital bispectral analysis and its applications to nonlinear wave interactions. *Plasma Science, IEEE Transactions on* 7: 120-131, 1979.

bioRxiv preprint doi: https://doi.org/10.1101/422246; this version posted September 19, 2018. The copyright holder for this preprint (which was not certified by peer review) is the author/funder, who has granted bioRxiv a license to display the preprint in perpetuity. It is made available under aCC-BY-NC-ND 4.0 International license.

Knight RT, and Eichenbaum H. Multiplexed memories: a view from human cortex. *Nat Neurosci* 16: 257-258, 2013.

Kocsis B, Bragin A, and Buzsáki G. Interdependence of multiple theta generators in the hippocampus: a partial coherence analysis. *J Neurosci* 19: 6200-6212, 1999.

Konopacki J, MacIver MB, Bland BH, and Roth SH. Carbachol-induced EEG 'theta' activity in hippocampal brain slices. *Brain Res* 405: 196-198, 1987.

Kropff E, Carmichael JE, Moser MB, and Moser EI. Speed cells in the medial entorhinal cortex. *Nature* 523: 419-424, 2015.

Lasztóczi B, and Klausberger T. Hippocampal Place Cells Couple to Three Different Gamma Oscillations during Place Field Traversal. *Neuron* 91: 34-40, 2016.

Leung LS. Fast (beta) rhythms in the hippocampus: a review. *Hippocampus* 2: 93-98, 1992.

Leung LS. Theta rhythm during REM sleep and waking: correlations between power, phase and frequency. *Electroencephalogr Clin Neurophysiol* 58: 553-564, 1984.

Li X, Li D, Voss LJ, and Sleigh JW. The comodulation measure of neuronal oscillations with general harmonic wavelet bicoherence and application to sleep analysis. *Neuroimage* 48: 501-514, 2009.

Lisman JE, and Jensen O. The θ-γ neural code. *Neuron* 77: 1002-1016, 2013.

Longuet-Higgins MS. Capillary rollers and bores. *Journal of Fluid Mechanics* 240: 659-679, 1992.

Lopez-Madrona VJ, Alvarez-Salvado E, Moratal D, Herreras O, Pereda E, Mirasso CR, and Canals S. Gamma oscillations coordinate different theta rhythms in the hippocampus. *bioRxiv* 418434, 2018.

Maurer AP, Burke SN, Lipa P, Skaggs WE, and Barnes CA. Greater running speeds result in altered hippocampal phase sequence dynamics. *Hippocampus* 22: 737-747, 2012.

Maurer AP, Cowen SL, Burke SN, Barnes CA, and McNaughton BL. Phase precession in hippocampal interneurons showing strong functional coupling to individual pyramidal cells. *J Neurosci* 26: 13485-13492, 2006.

Maurer AP, Vanrhoads SR, Sutherland GR, Lipa P, and McNaughton BL. Self-motion and the origin of differential spatial scaling along the septo-temporal axis of the hippocampus. *Hippocampus* 15: 841-852, 2005.

McLelland D, and VanRullen R. Theta-Gamma Coding Meets Communication-through-Coherence: Neuronal Oscillatory Multiplexing Theories Reconciled. *PLoS Comput Biol* 12: e1005162, 2016.

McNaughton BL, Barnes CA, and O'Keefe J. The contributions of position, direction, and velocity to single unit activity in the hippocampus of freely-moving rats. *Exp Brain Res* 52: 41-49, 1983.

Mitzdorf U. Current source-density method and application in cat cerebral cortex: investigation of evoked potentials and EEG phenomena. *Physiol Rev* 65: 37-100, 1985.

Montgomery SM, Sirota A, and Buzsáki G. Theta and gamma coordination of hippocampal networks during waking and rapid eye movement sleep. *J Neurosci* 28: 6731-6741, 2008.

Moser EI, and Moser MB. A metric for space. *Hippocampus* 18: 1142-1156, 2008.

Muthuswamy J, Sherman DL, and Thakor NV. Higher-order spectral analysis of burst patterns in EEG. *IEEE Trans Biomed Eng* 46: 92-99, 1999.

Ning TK, and Bronzino JD. Bispectral analysis of the rat EEG during various vigilance states. *IEEE Trans Biomed Eng* 36: 497-499, 1989.

Papoulis A, and Pillai SU. *Probability, random variables, and stochastic processes*. Tata McGraw-Hill Education, 2002.

Penttonen M, Kamondi A, Acsády L, and Buzsáki G. Gamma frequency oscillation in the hippocampus of the rat: intracellular analysis in vivo. *Eur J Neurosci* 10: 718-728, 1998.

Pikkarainen M, Rönkkö S, Savander V, Insausti R, and Pitkänen A. Projections from the lateral, basal, and accessory basal nuclei of the amygdala to the hippocampal formation in rat. *J Comp Neurol* 403: 229-260, 1999.

bioRxiv preprint doi: https://doi.org/10.1101/422246; this version posted September 19, 2018. The copyright holder for this preprint (which was not certified by peer review) is the author/funder, who has granted bioRxiv a license to display the preprint in perpetuity. It is made available under aCC-BY-NC-ND 4.0 International license.

Plenz D, and Thiagarajan TC. The organizing principles of neuronal avalanches: cell assemblies in the cortex? *Trends Neurosci* 30: 101-110, 2007.

Pradhan C, Jena SK, Nadar SR, and Pradhan N. Higher-order spectrum in understanding nonlinearity in EEG rhythms. *Comput Math Methods Med* 2012: 206857, 2012.

Priestley MB. Spectral analysis and time series. 1981.

Rappelsberger P, Pockberger H, and Petsche H. Current source density analysis: methods and application to simultaneously recorded field potentials of the rabbit's visual cortex. *Pflugers Arch* 389: 159-170, 1981.

Sargolini F, Fyhn M, Hafting T, McNaughton BL, Witter MP, Moser MB, and Moser EI. Conjunctive representation of position, direction, and velocity in entorhinal cortex. *Science* 312: 758-762, 2006.

Scheffer-Teixeira R, and Tort AB. On cross-frequency phase-phase coupling between theta and gamma oscillations in the hippocampus. *Elife* 5: 2016.

Schomburg EW, Fernández-Ruiz A, Mizuseki K, Berényi A, Anastassiou CA, Koch C, and Buzsáki G. Theta Phase Segregation of Input-Specific Gamma Patterns in Entorhinal-Hippocampal Networks. *Neuron* 2014.

Shahbazi Avarvand F, Bartz S, Andreou C, Samek W, Leicht G, Mulert C, Engel AK, and Nolte G. Localizing bicoherence from EEG and MEG. *Neuroimage* 174: 352-363, 2018.

Sheremet A, Burke SN, and Maurer AP. Movement Enhances the Nonlinearity of Hippocampal Theta. *J Neurosci* 36: 4218-4230, 2016.

Shik M, Severin F, and Orlovsky G. Control of walking and running by means of electrical stimulation of the mesencephalon. *Electroencephalography and clinical neurophysiology* 26: 549-549, 1969.

Siegel M, Donner TH, and Engel AK. Spectral fingerprints of large-scale neuronal interactions. *Nat Rev Neurosci* 13: 121-134, 2012.

Sigl JC, and Chamoun NG. An introduction to bispectral analysis for the electroencephalogram. *Journal of clinical monitoring* 10: 392-404, 1994.

Skaggs WE, McNaughton BL, Wilson MA, and Barnes CA. Theta phase precession in hippocampal neuronal populations and the compression of temporal sequences. *Hippocampus* 6: 149-172, 1996.

Stark E, Eichler R, Roux L, Fujisawa S, Rotstein HG, and Buzsáki G. Inhibition-induced theta resonance in cortical circuits. *Neuron* 80: 1263-1276, 2013.

Stumpf C. Drug action on the electrical activity of the hippocampus. *Int Rev Neurobiol* 8: 77-138, 1965.

Sullivan D, Csicsvari J, Mizuseki K, Montgomery S, Diba K, and Buzsáki G. Relationships between hippocampal sharp waves, ripples, and fast gamma oscillation: influence of dentate and entorhinal cortical activity. *J Neurosci* 31: 8605-8616, 2011.

Swami A, Mendel J, and Nikias C. HOSA-Higher order spectral analysis toolbox. *MATLAB CENTRAL* 2003.

Terrazas A, Krause M, Lipa P, Gothard KM, Barnes CA, and McNaughton BL. Self-motion and the hippocampal spatial metric. *J Neurosci* 25: 8085-8096, 2005.

Tort AB, Komorowski RW, Manns JR, Kopell NJ, and Eichenbaum H. Theta-gamma coupling increases during the learning of item-context associations. *Proc Natl Acad Sci U S A* 106: 20942-20947, 2009.

Tort AB, Kramer MA, Thorn C, Gibson DJ, Kubota Y, Graybiel AM, and Kopell NJ. Dynamic cross-frequency couplings of local field potential oscillations in rat striatum and hippocampus during performance of a T-maze task. *Proc Natl Acad Sci U S A* 105: 20517-20522, 2008.

Tropp J, Figueiredo CM, and Markus EJ. Stability of hippocampal place cell activity across the rat estrous cycle. *Hippocampus* 15: 154-165, 2005.

Vaidya SP, and Johnston D. Temporal synchrony and gamma-to-theta power conversion in the dendrites of CA1 pyramidal neurons. *Nat Neurosci* 16: 1812-1820, 2013.

Van Milligen BP, Sanchez E, Estrada T, Hidalgo C, Brañas B, Carreras B, and Garcia L. Wavelet bicoherence: a new turbulence analysis tool. *Physics of Plasmas* 2: 3017-3032, 1995.

bioRxiv preprint doi: https://doi.org/10.1101/422246; this version posted September 19, 2018. The copyright holder for this preprint (which was not certified by peer review) is the author/funder, who has granted bioRxiv a license to display the preprint in perpetuity. It is made available under aCC-BY-NC-ND 4.0 International license.

Vandecasteele M, M S, Royer S, Belluscio M, Berényi A, Diba K, Fujisawa S, Grosmark A, Mao D, Mizuseki K, Patel J, Stark E, Sullivan D, Watson B, and Buzsáki G. Large-scale recording of neurons by movable silicon probes in behaving rodents. *J Vis Exp* e3568, 2012.

Vanderwolf CH. Hippocampal electrical activity and voluntary movement in the rat. *Electroencephalogr Clin Neurophysiol* 26: 407-418, 1969.

Wang J, Fang Y, Wang X, Yang H, Yu X, and Wang H. Enhanced Gamma Activity and Cross-Frequency Interaction of Resting-State Electroencephalographic Oscillations in Patients with Alzheimer's Disease. *Front Aging Neurosci* 9: 243, 2017.

Wang XJ, and Buzsáki G. Gamma oscillation by synaptic inhibition in a hippocampal interneuronal network model. *J Neurosci* 16: 6402-6413, 1996.

Watrous AJ, Tandon N, Conner CR, Pieters T, and Ekstrom AD. Frequency-specific network connectivity increases underlie accurate spatiotemporal memory retrieval. *Nat Neurosci* 16: 349-356, 2013.

Winson J. Loss of hippocampal theta rhythm results in spatial memory deficit in the rat. *Science* 201: 160-163, 1978.

Witter MP, Griffioen AW, Jorritsma-Byham B, and Krijnen JL. Entorhinal projections to the hippocampal CA1 region in the rat: an underestimated pathway. *Neurosci Lett* 85: 193-198, 1988.

Wouterlood FG, Saldana E, and Witter MP. Projection from the nucleus reuniens thalami to the hippocampal region: light and electron microscopic tracing study in the rat with the anterograde tracer Phaseolus vulgaris-leucoagglutinin. *J Comp Neurol* 296: 179-203, 1990.

Ylinen A, Bragin A, Nádasdy Z, Jandó G, Szabó I, Sik A, and Buzsáki G. Sharp wave-associated high-frequency oscillation (200 Hz) in the intact hippocampus: network and intracellular mechanisms. *J Neurosci* 15: 30-46, 1995a.

Ylinen A, Soltész I, Bragin A, Penttonen M, Sik A, and Buzsáki G. Intracellular correlates of hippocampal theta rhythm in identified pyramidal cells, granule cells, and basket cells. *Hippocampus* 5: 78-90, 1995b.

Zheng C, Bieri KW, Trettel SG, and Colgin LL. The relationship between gamma frequency and running speed differs for slow and fast gamma rhythms in freely behaving rats. *Hippocampus* 25: 924-938, 2015.